Current Climate Change Reports (2025) 11:6
https://doi.org/10.1007/s40641-025-00203-4

REVIEW

Three Paradoxes Related to Potential Evapotranspiration in a Warming Climate

Kaiwen Wang[1] · Peng Bai[1] · Xiaomang Liu[1]

Accepted: 26 May 2025

Abstract

Purpose of review We review three intriguing paradoxes related to potential evapotranspiration in a warming climate: global 'evaporation, aridity, and drought paradoxes'.

Recent findings The 'evaporation paradox' is the contradiction between the expected increase in atmospheric evaporative demand and the observed decrease in its proxy—pan evaporation. The 'aridity (drought) paradox' refers to the conflicting perspectives on whether terrestrial aridification (drought) intensifies or mitigates under global warming.

Summary Before the mid-1990s, the enhancing effect of rising air temperature on pan evaporation is outweighed by the weakening effects of reduced shortwave radiation and wind speed, leading to a decrease in global mean pan evaporation and the emergence of the 'evaporation paradox'. After that, rising air temperature and radiation drive an upward trend in pan evaporation, causing the paradox to disappear. We validate the deduction that neglecting stomatal responses in traditional potential evapotranspiration calculations is a key factor underlying the 'aridity paradox'. For the 'drought paradox', this neglect explains the paradoxical trends in drought indices but fails for drought extent and frequency.

Keywords Potential Evapotranspiration · 'Evaporation Paradox' · 'Aridity Paradox' · 'Drought Paradox'

Introduction

Anthropogenic climate warming is expected to influence the global hydrological cycle, complicating the formation and evolution of terrestrial water resources and posing challenges to their sustainable use [1]. In examining the response of the global hydrological cycle to climate warming, three paradoxes—evaporation, aridity, and drought paradoxes—have sparked extensive discussion. The 'evaporation paradox' is the contradiction between the expected increase in atmospheric evaporative demand (*AED*) and the observed decrease in its observational proxy, pan evaporation [2]. The 'aridity paradox' and 'drought paradox' refer to the conflicting perspectives on whether terrestrial aridification and drought are intensifying or mitigating under global warming [3, 4].

Though these paradoxes stem from various factors—including uncertainties in forcing data, differences in methods, and divergencies in analytical views—their explanations are interlinked and are all related to potential evapotranspiration (*PET*) [5]. Specifically, pan evaporation, central to studies of the 'evaporation paradox', approximates the *PET* under the condition that water vapor escapes from an open-water surface with zero resistance [6]. In contrast, aridity and drought are quantified using *PET* that accounts for stomatal friction to water vapor, introducing extra resistance compared to pan evaporation [7]. In this light, we review the emergence, development, and potential explanations of these paradoxes from the perspective of *PET*, aiming to explore and compare the differentiated responses of *AED*, aridity, and drought to climate warming when accounting for *PET* with different levels of resistance quantifications.

The 'evaporation paradox' involves distinguishing between evaporation, *AED*, and *PET*. Evaporation—also known as evapotranspiration [8]—represents the phase transition of water from liquid to gas at the surface and its

✉ Peng Bai
baip@igsnrr.ac.cn

[1] Key Laboratory of Water Cycle and Related Land Surface Processes, Institute of Geographic Sciences and Natural Resources Research, Chinese Academy of Sciences, Beijing, China

Published online: 07 June 2025

subsequent transfer to the atmosphere [9]. On the contrary, *AED* does not correspond to a land–atmosphere flux but to the water demand from the atmosphere [10]. *AED* is generally approximated by *PET*, which refers to the theoretical maximum evapotranspiration that could occur given unlimited water availability at the surface [11]. Broadly, pan evaporation (water evaporated from a metal pan), open-water evaporation, and reference crop evapotranspiration can be deemed as the approximation of *PET*. *PET* requires only meteorological observations for estimation and is therefore broadly applied in aridity assessment and drought monitoring [12–16]. Physically, *AED* and *PET* are driven by two types of forces: (1) radiative forcing, which provides the energy needed for water vaporization and is largely governed by surface net radiation, and (2) aerodynamic forcing, which determines moisture-holding capacity in the air, primarily influenced by air temperature, wind speed, and humidity [10]. As greenhouse gases continue to be emitted and accumulate, the resultant increases in terrestrial net radiation and atmospheric moisture capacity are expected to elevate *AED*. However, studies based on extensive pan evaporation observations, as well as global open-water evaporation and reference crop evapotranspiration calculations, reported decreasing trends before the mid-1990s [2, 17–19]. Thus, the expected increasing trends of *AED* versus counter-intuitive decreasing trends in its proxies are concluded as the 'evaporation paradox'.

Aridity is a permanent climate feature of a region representing a long-term state of water scarcity. It is commonly quantified by the aridity index (*AI*), which is the ratio of the long-term average of water supply or precipitation to the long-term average of *PET* [13]. Based on this index, the latest World Atlas of Desertification publicized by the European Commission Joint Research Centre [20] classifies global climate into drylands ($AI < 0.65$) and humid lands ($AI > 0.65$). By using reference crop evapotranspiration to represent *PET*, numerous studies reported exacerbating aridification and expanding drylands during historical periods and under future climate scenarios [20–23]. In contrast, observed 'vegetation greening', projected runoff increasing, and paleoclimate-reconstructed declines in the dust during the warmer interglacial periods suggest a contrasting narrative: attenuating aridification and shrinking drylands in a warming climate [3, 7, 24]. To our best knowledge, Roderick et al. first introduced the term 'aridity paradox' to describe such conflicting aridification estimates [7]. They suggested that these discrepancies may arise from neglecting stomatal responses in the calculation of reference crop evapotranspiration—specifically, assuming a fixed stomatal aperture and resistance, as quantified in Sect. Penman-Monteith Reference Crop (PM-RC) Model. Indeed, plant stomata are influenced by multiple environmental variables. In a warming climate, increasing atmospheric CO_2 concentration and vapor pressure deficit (the difference between the saturated vapor pressure and the actual vapor pressure), together with decreasing soil moisture, tend to induce stomatal closure to reduce water loss through transpiration. Rising air temperature and radiation promote stomatal opening to protect leaves from irreversible heat damage via evaporative cooling and to enhance photosynthesis. To quantify the impact of neglecting stomatal responses on aridity calculations, Yang et al. modified the reference crop evapotranspiration by incorporating a linear relationship between stomata and CO_2 concentration [6], which implicitly lumps other environmental influences on stomata as ultimately caused by CO_2 concentration. Utilizing this modification, previous drying *AI* projections are alleviated [25], while the exacerbating aridification remains unchanged (the same result has been reported using many other *PET* formulas) [26, 27]. Given the severe consequences of exacerbating aridification [22], it is essential to further investigate stomatal responses to changing environmental variables to reconcile the conflicting aridification estimates.

Unlike aridity, droughts represent short-term water deficits relative to average baseline conditions and are typically classified into meteorological, agricultural, and hydrological categories [28, 29]. Most droughts originate from anomalously low precipitation, referred to as meteorological droughts. Prolonged precipitation deficits can further lead to reduced soil moisture (agricultural droughts) and declining runoff, streamflow, surface reservoir levels, and groundwater supplies (hydrological droughts) [30, 31]. Droughts are quantified using various indices, many of which rely on *PET*, such as the widely used Palmer Drought Severity Index (*PDSI*) [32] and Standardized Precipitation Evapotranspiration Index (*SPEI*) [33]. By using reference crop evapotranspiration in the calculations of *PDSI* and *SPEI*, these indices exhibit decreasing trends, suggesting exacerbating drought conditions both historically and under different future trajectories [34–37]. In contrast, some studies reported limited changes or great uncertainties in the evolution of droughts [38]. Trenberth et al. concluded that differences in *PET* formulas and their forcing data possibly contribute to these paradoxical results [4]. Existing studies on the 'drought paradox' primarily focus on global average changes in drought indices [4, 38, 39], which serve as proxies for global mean drought conditions. However, beyond what is reflected by the changes in drought indices, droughts also involve other important characteristics, such as frequency, duration, and spatial extent [40, 41]. Since droughts are the most expensive and damaging climate extremes globally [11], it is crucial to examine whether different *PET* formulas affect the temporal changes in other characteristics [4, 39].

The rest of the paper is organized as follows. Section Evaporation Paradox reviews the development of physical pan evaporation models, explains the decline in pan evaporation under global warming before the mid-1990s, namely the emergence of the 'evaporation paradox', using these models, and demonstrates the increase in pan evaporation after the mid-1990s, i.e., the disappearance of the paradox. Next, we review the influence of different stomatal responses in *PET* calculations on the 'aridity paradox' and 'drought paradox'. In Sect. Accounting for stomatal responses in PET, we introduce *PET* calculations that neglect stomatal responses (Sect. Penman-Monteith Reference Crop (PM-RC) Model), account for the influence of CO_2 concentration (Sect. Accounting for the Stomatal Response to Rising [CO_2]), and consider diverse environmental factors (Sect. Accounting for Stomatal Responses to Diverse Environmental Factors). Based on these methods, we discuss the impact of neglecting stomatal responses on the 'aridity paradox' in Sect. Aridity Paradox, and on the 'drought paradox' in Sect. Drought Paradox.

Evaporation Paradox

Explaining the 'evaporation paradox' necessitates a physical clarification of why pan evaporation decreases in a warming climate. Consequently, multiple models have been developed to quantify the physical processes governing the pan evaporation. Thom et al. developed a Penman-style model [42] and Pereira et al. derived a Penman-Monteith style model [43], which quantifies aerodynamic influence on pan evaporation using standard meteorological measurements at 2 m above ground. Linacre improved the radiative quantification of previous models and derived the Penpan model [44]. By combining the aerodynamic component from Thom's method with the radiative component of the Penpan model, Rotstayn et al. developed the PenPan model [45] (note the two capital Ps to differentiate it from Linacre's "Penpan"). Lim et al. developed the PenPan-V2 model by systematically quantifying vapor transfer between the water surface and atmosphere, heat transfer in boundary layers, and the radiation processes affecting the pan's water surface and walls [46]. All the above models are specifically designed for the US Class A pan. Though the US Class A pan is widely used in many countries, the Russian GGI-3000, China D20, and China 601B pans also have extensive regional coverage. However, these pans are made with different specifications and materials, resulting in slightly varied physical processes of pan evaporation [47, 48]. Considering these differences, Wang et al. derived the generalized PenPan-V3 model, which can simulate the evaporation of different pans [49].

Forcing by standard meteorological observations, such as wind speed, air temperature, and downwelling radiation, the above physical models agree on the underlying causes of decreasing pan evaporation before the mid-1990s. Specifically, before that, the enhancing effect of rising air temperature (global warming) and vapor pressure deficit on pan evaporation is outweighed by the weakening effects of reduced short-wave radiation (global dimming [50]) and declined wind speed (global stilling [51]) [52, 53]. With the acceleration of global warming [54], the reversal of global stilling [55], and the transition from global dimming to brightening [56, 57] after the mid-1990s, the pan evaporation increased across most regions globally [58–61]. This suggests that the evaporation paradox no longer exists; in other words, the paradox has disappeared. To analyze the emergence and disappearance of the 'evaporation paradox', we use CMIP6 monthly meteorological outputs (Fig. 1a) to calculate monthly pan evaporation, which is then aggregated into yearly anomalies for four widely used pans, namely US Class A, Russian GGI-3000, China D20, and China 601B pans. Due to the systematic bias between CMIP6 outputs and observational data, CMIP6 simulated meteorological data are post-processed using bias correction methods. Here, we use outputs from 26 CMIP6 models (ACCESS-CM2, ACCESS-ESM1-5, BCC-CSM2-MR, CanESM5, CanESM5-CanOE, CESM2, CESM2-WACCM, CNRM-CM6-1, CNRM-ESM2-1, EC-Earth3, EC-Earth3-Veg, FGOALS-f3-L, FGOALS-g3, GFDL-ESM4, GISS-E2-1-G, HadGEM3-GC31-LL, INM-CM4-8, INM-CM5-0, IPSL-CM6A-LR, MIROC6, MIROC-ES2L, MPI-ESM1-2-HR, MPI-ESM1-2-LR, MRI-ESM2-0, NorESM2-MM, and UKESM1-0-LL) mainly for the climatological analysis, which indicates ensuring the variable accuracy over a long period is our top priority. For example, the analysis of *AI* requires the accuracy of mean precipitation and *PET* over a long period. Therefore, we used a mean-based bias correction method, which estimates the bias as the difference (or ratio) between simulated and observed mean over a reference period, and adjusts the simulated time series over a scenario period with the help of the estimated bias (by adding or rescaling it). We use the Princeton Global Meteorological Forcing Dataset [62] as the benchmark for bias correction because (1) it ensures consistency across multiple climatic variables, and (2) it has been widely applied and validated in modeling and analyzing land surface processes, including aridity and drought assessments.

Before the mid-1990s, increasing air temperature and downwelling longwave radiation would enhance the pan evaporation, whereas decreasing downwelling shortwave radiation and wind speed would weaken it. The decreasing pan evaporation before the mid-1990s (Fig. 1b) results from the weakening effects outweighing the enhancing effects,

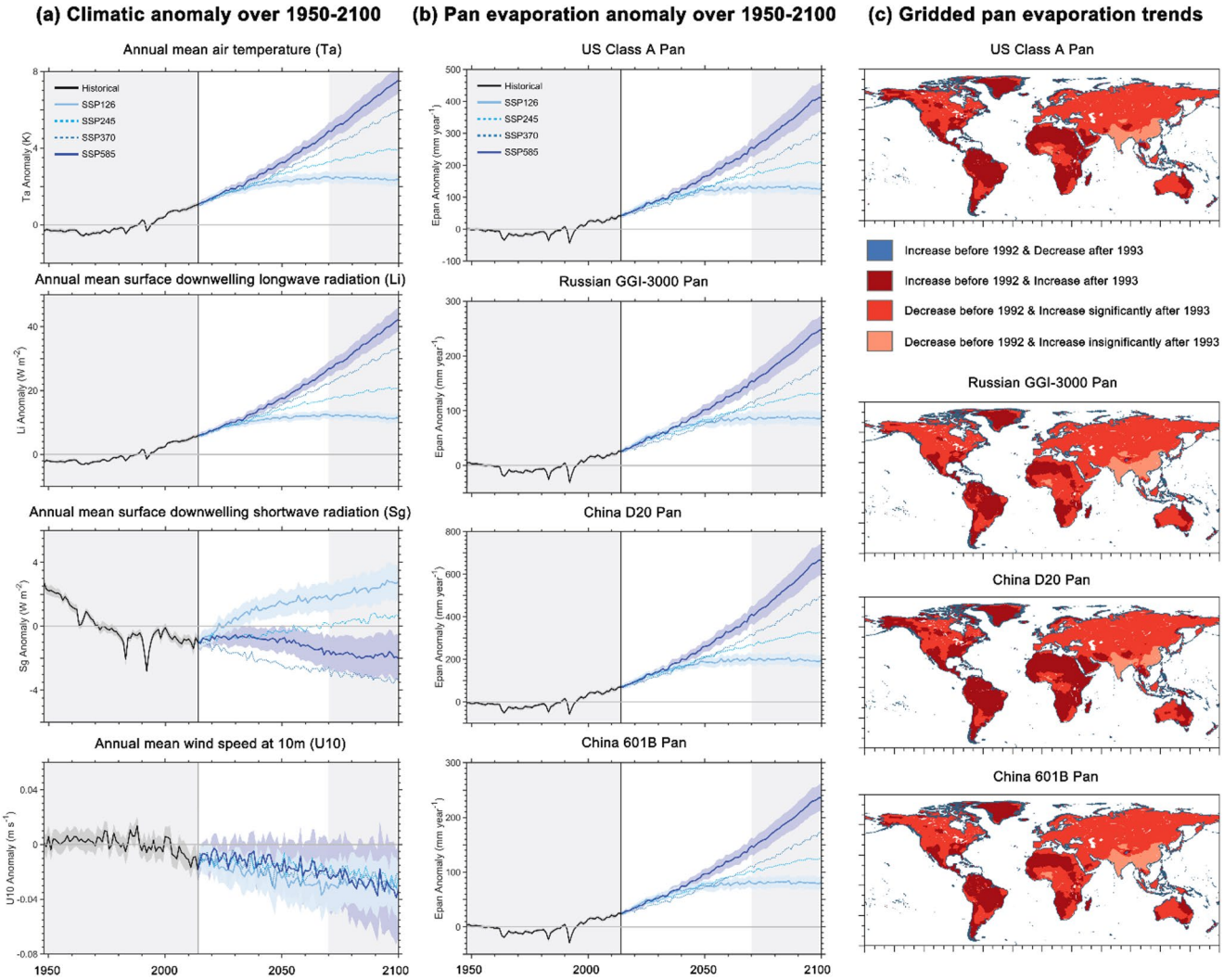

Fig. 1 Spatiotemporal characteristics of global pan evaporation and associated climatic influencing variables. **a**, climatic anomalies over 1950–2100 relative to 1950–2014 mean calculated using CMIP6 historical outputs (black lines), and SSPs 126, 245, 370, 585 future scenarios (blue lines). Solid lines represent annual values mean over 26 CMIP6 models. The shading is the 95% confidence intervals of 26 CMIP6 models. Two grey rectangular areas represent two time periods: 1950–2014 and 2070–2100. **b**, 1950–2100 pan evaporation anomalies relative to 1950–2014 mean. **c**, gridded pan evaporation trends before 1992 and after 1993. Linear trends with P values <0.05 and >0.05 are respectively marked as significant and insignificant

which contributes to the emergence of the 'evaporation paradox'. As climate warming continues after the mid-1990s, rising air temperature and downwelling longwave radiation are projected to drive upward trends in pan evaporation (Fig. 1a and b), indicating the disappearance of the paradox.

To illustrate the spatial distribution of the emergence and disappearance of the 'evaporation paradox', we analyze pan evaporation trends before and after 1992. Figure 1c shows that the pan evaporation decreases across vast areas of the Northern Hemisphere, Australia, and central Africa before 1992, indicating the emergence of the paradox, yet shifts to an increasing trend afterward, signifying its disappearance. Differently, across large regions of South America and North Africa, pan evaporation exhibits an increasing trend in both the pre-1992 and post-1993 periods, indicating that the paradox does not emerge in these regions. The absence of decreasing pan evaporation after 1993 in Fig. 1c indicates that the 'evaporation paradox' is unlikely to recur in a warming climate. It is worth noting that gridded pan evaporation trends before and after 1991, 1993, and 1994 exhibit spatial patterns similar to those of 1992. Thus, the above spatial distribution of the emergence and disappearance of the 'evaporation paradox' applies to the period before and after the mid-1990s.

Accounting for Stomatal Responses in *PET*

To quantify the impact of neglecting stomatal responses to environmental changes in *PET* calculations on the 'aridity paradox' and 'drought paradox', we introduce different formulas of *PET* before analyzing these paradoxes. *PET* is widely estimated using the Penman-Monteith reference crop equation, which defines extensively-distributed and well-watered plants with specific characteristics as the reference crop [63]. This equation assumes a fixed stomatal resistance (r_l) of 100 s/m, implying constant friction of the vapor flowing through the fixed stomatal aperture [63]. In a CO_2-enriched future, however, this assumption would be incorrect, since plant leaves would partially close their stomata and reduce transpiration with atmospheric CO_2 concentration ([CO_2]) rising [7]. To correct this, Yang et al. modified the Penman-Monteith reference crop Eq. (3) by introducing a linear relationship between [CO_2] and surface resistance, which is the scale-down of r_l.

In addition to elevated [CO_2], plant stomata are influenced by various environmental factors, which have counteracting effects on r_l [64]. In a warming climate, with [CO_2] and vapor pressure deficit increasing, plant leaves partially close their stomata to reduce the amount of water loss through transpiration. Conversely, with air temperature and radiation climbing, plants tend to keep stomata open to protect their leaves from irreversible heat damage through evaporative cooling and to enhance photosynthesis [65]. More complicated, current air temperatures appear to be near or above the optimum for photosynthesis in some places, and future warming would reversely lead to stomatal closure [3]. In this light, using ecological stomatal formulas to modify the reference crop equation is indispensable to unravel the 'aridity paradox' and 'drought paradox'. In the following subsections, we review the reference crop equation (Sect. Penman-Monteith Reference Crop (PM-RC) Model) and Yang's modification (Sect. Accounting for the Stomatal Response to Rising [CO_2]), and propose a new modification that accounts for stomatal responses to diverse environmental factors (Sect. Accounting for Stomatal Responses to Diverse Environmental Factors), shedding light on the methodological artifacts underlying these paradoxes.

Penman-Monteith Reference Crop (PM-RC) Model

PM-RC model is derived from the Penman-Monteith model [63], which is accepted as the most comprehensive approach to calculate evapotranspiration (*ET*, mm day^{-1}):

$$ET = \frac{1}{\lambda}\frac{sR_n^* + 86400\rho_a C_a VPD/r_a}{s+\gamma\left(1+\frac{r_s}{r_a}\right)} \quad (1)$$

in which λ (MJ kg^{-1}) is the latent heat of vaporization; γ (kPa ^{o}C^{-1}) is the psychrometric constant; s (kPa ^{o}C^{-1}) is the slope of the plot of saturated vapor pressure against air temperature (T_a, ^{o}C) at 2 m above the ground; ρ_a (kg m^{-3}) and C_a (MJ kg^{-1}^{o}C^{-1}) are air density and specific heat at constant pressure; R_n^*(MJ m^{-2}day^{-1}) and *VPD* (kPa) are the available energy (that is equal to net irradiance minus ground heat flux) and vapor pressure deficit at 2 m; r_a (s m^{-1}) is the aerodynamic resistance; and r_s (s m^{-1}) is the surface resistance. Based on the Penman-Monteith model, the Food and Agriculture Organization derived the PM-RC model, which defines the extensively-distributed and well-watered green grass as the reference crop. In the derivation of the PM-RC model, r_s in Eq. (1) is specified as:

$$r_s = \frac{r_l}{LAI_a} \quad (2)$$

where r_l (s m^{-1}) is stomatal resistance; and LAI_a is the active leaf area index and can be estimated by (0.5×24×crop height). Besides, the PM-RC model is derived by fixing crop height, r_l, and r_s to 0.12 m, 100 s m^{-1}, and 70 s m^{-1}, which represents an extensive surface of reference crop with uniform height and constant frictions of the vapor flowing through the stomata and canopy. The uniform height assumption implies r_l is the 1.44 (=0.5×24×0.12) times scale-up of r_s additionally considering the fixed canopy resistance of the reference crop. According to the derivation and calculation guidelines given by the Food and Agriculture Organization [63], reference crop evapotranspiration (ET_{rc}, mm day^{-1}) is calculated as:

$$ET_{rc} = \frac{0.408sR_n^* + \gamma\frac{900}{T_a+273}WS_2VPD}{s+\gamma\left(1+0.34WS_2\right)} \quad (3)$$

where WS_2 (m s^{-1}) represents wind speed at 2 m.

Accounting for the Stomatal Response to Rising [CO_2]

Hypothesizing fixed r_l and r_s in PM-RC model results in the calculated *PET* ignoring stomatal responses to the changing environment. To incorporate the stomatal responses under rising [CO_2], Yang et al. lumped all factors influencing r_s as ultimately caused by CO_2, and regressed a linear equation between relative changes of r_s and [CO_2] from CMIP5 model output:

$$r_s = r_{s\_300} + 0.05 \times ([CO_2] - 300) \quad (4)$$

where r_{s_300} is equal to 70 s/m, representing the surface resistance when [CO_2] is 300 ppm [6]. By introducing

Eq. (4) into PM-RC model, reference crop evapotranspiration is modified (denoted as $ET_{rc-Yang}$, mm day^{-1}) with [CO_2] as a new independent variable [6]:

$$ET_{rc-Yang} = \frac{0.408sR_n^* + \gamma \frac{900}{T_a+273} WS_2 VPD}{s + \gamma \left\{1 + WS_2 \left[0.34 + 2.4 \times 10^{-4} \left([CO_2] - 300\right)\right]\right\}} \quad (5)$$

It is noteworthy that Eq. (4) is derived from a wide range of natural vegetation rather than specifically designed for the grass-like reference crop, since r_s is quantified by inverting the Penman-Monteith model with the help of CMIP5 evapotranspiration outputs [6], which represents evapotranspiration of various vegetation types, including forest, savannah, grassland, etc. Thus, introducing the relationship derived from various vegetation types may not strictly represent the reference crop.

Accounting for Stomatal Responses to Diverse Environmental Factors

In addition to [CO_2], plant stomata are influenced by various environmental factors. To integrate stomatal responses to diverse environmental factors, Jarvis proposed a multiplicative method to simulate r_l [66]. Jarvis-type stomatal model (Eq. (6)) scales up the minimum r_l (r_{lmin}) with the product of empirical weighting functions associated with multiple environmental factors, and is widely used by early Earth system models. Here, we introduce Eq. (6) to modify the PM-RC model for quantifying the environmental influences on stomata.

$$r_l = \frac{r_{lmin}}{LAI} f^{-1}(S_g) f^{-1}(T_a) f^{-1}(VPD) f^{-1}(\theta) f^{-1}([CO_2]) \quad (6)$$

where $f(S_g)$, $f(T_a)$, $f(VPD)$, $f(\theta)$ and f([CO_2]) are weighting functions varying between 0 and 1 to represent the effects of plant stress due to global solar radiation (S_g, W m^{-2}), T_a, VPD, soil moisture (θ) and [CO_2] (ppm), respectively. According to the derivation and calculation guidelines of the PM-RC model, $f(\theta)$ can be set to 1, as the reference crop does not have water stress; and LAI in Eq. (6) can be calculated by 24×crop height. The parameterization scheme of $f(S_g)$, $f(T_a)$, and $f(VPD)$ implemented in the early Earth system models for grass and irrigated crop [67, 68] is used:

$$f(S_g) = \frac{\frac{r_{lmin}}{r_{lmax}} + 0.55 \times \frac{2S_g}{S_{gl} LAI}}{1 + 0.55 \times \frac{2S_g}{S_{gl} LAI}} \quad (7)$$

$$f(T_a) = 1 - 0.0016 \times (298 - 273.15 - T_a)^2 \quad (8)$$

$$f(VPD) = 1 - 0.025 \times VPD \quad (9)$$

where r_{lmax} is the maximum r_l (=5000 s m^{-1}), S_{gl} is the minimum S_g necessary for transpiration to occur (=100 W m^{-2}), and r_{lmin} can be set as 100 s m^{-1}, since this value represents the resistance under little environmental stress according to original reference crop assumptions [63]. Early Earth system models using Eq. (6) ignore the effects of [CO_2] on stomata by assuming f([CO_2])=1, here, we adopt the parameterization scheme of f([CO_2]) provided by Jarvis [66]:

$$f([CO_2]) = \begin{cases} 1 & [CO_2] \le 100ppm \\ 1 - \frac{1-x}{900}[CO_2] & 100ppm < [CO_2] < 1000ppm \\ x & [CO_2] \ge 1000ppm \end{cases} \quad (10)$$

where x is the weighting factor at the values of [CO_2] larger than 1000 ppm, and x is assigned to 0.9 in this study. Finally, introducing Eq. (6) into the PM-RC model gets,

$$ET_{rc-Jarvis} = \frac{0.408sR_n^* + \gamma \frac{900}{T_a+273} WS_2 VPD}{s + \gamma \begin{Bmatrix} 1 + 0.116WS_2 \times f^{-1}(S_g) f^{-1}(T_a) \\ f^{-1}(VPD) f^{-1}(\theta) f^{-1}([CO_2]) \end{Bmatrix}} \quad (11)$$

In Sects. Aridity Paradox and Drought Paradox, we calculate ET_{rc}, $ET_{rc-Yang}$, and $ET_{rc-Jarvis}$ using monthly meteorological data, which are then aggregated into yearly data to estimate aridity and drought indices.

Aridity Paradox

To assess the impact of neglecting stomatal responses on the 'aridity paradox', we calculate annual aridity indices, namely the ratio of precipitation to ET_{rc}, $ET_{rc-Yang}$, and $ET_{rc-Jarvis}$. Figures 2a-c left panels illustrate divergent aridity trajectories projected by different stomatal quantifications. Specifically, the aridity index calculated by ET_{rc} slightly decreases during the historical period, and sharply decreases (drying evolution) under future scenarios. The aridity index calculated by $ET_{rc-Yang}$ slightly increases during the historical period but shifts to downward trends in the future, with minimal variation across different emission scenarios. The aridity index calculated by $ET_{rc-Jarvis}$ shows a slight increase (wetting evolution) during the historical period, maintaining this gradual trend under low and medium greenhouse gas emission pathways (SSPs 126 and 245 scenarios). Yet, it rises rapidly under high emission pathways (SSPs 370 and 585 scenarios). These discrepancies indicate that neglecting stomatal responses leads to an overestimation of aridification, while considering the stomatal response to elevated [CO_2] would mitigate it. Accounting for stomatal responses to diverse environmental factors reveals a wetting tendency (increasing AI), which is consistent with the wetting

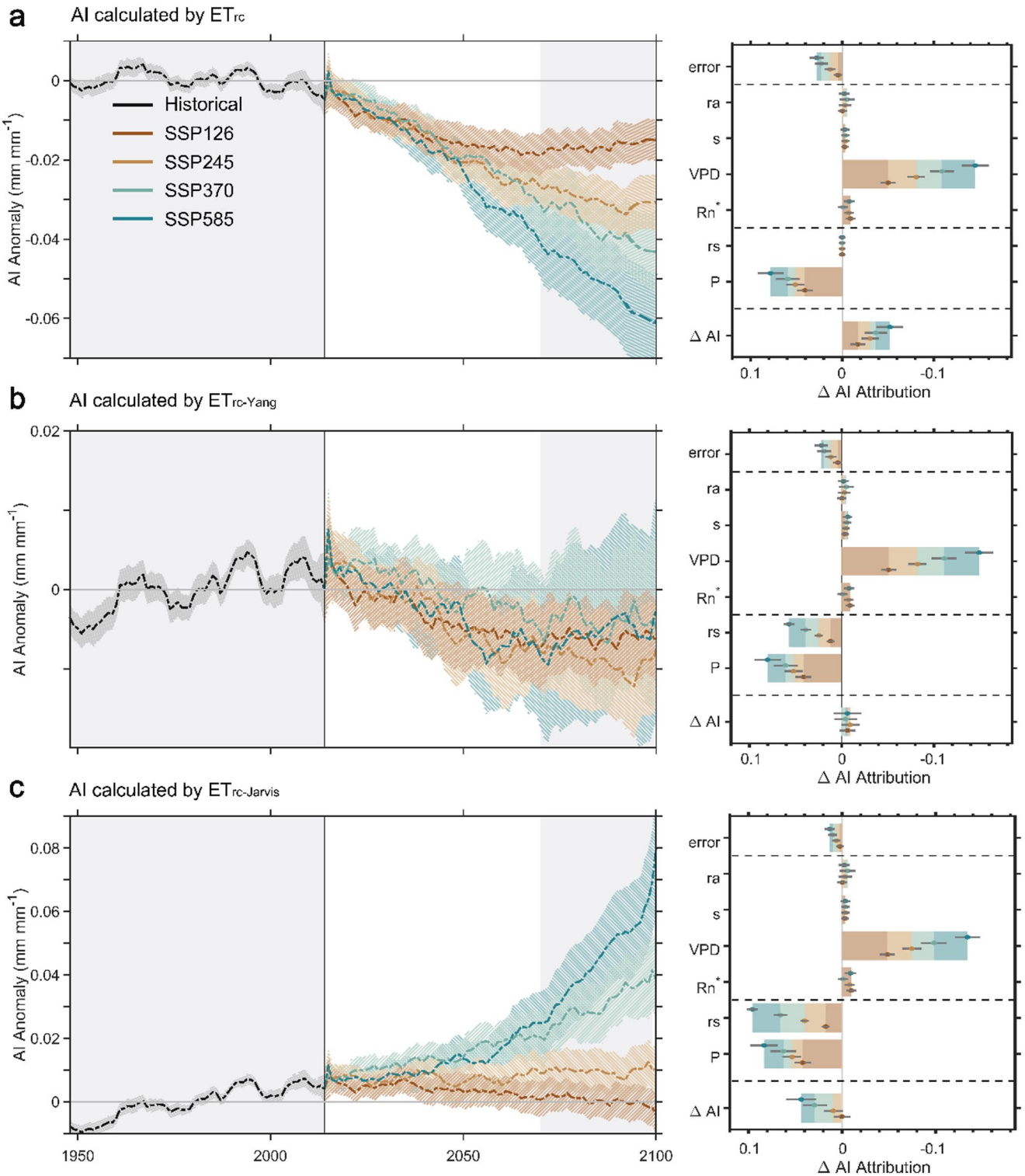

Fig. 2 Aridity index (*AI*) calculated by ET_{rc} (**a**), $ET_{rc-Yang}$ (**b**), and $ET_{rc-Jarvis}$ (**c**). The left panel in **a-c**, annual *AI* anomalies over 1950–2100 relative to 1950–2014 mean. *AI* is calculated using CMIP6 historical (1950–2014) outputs and SSPs future (2015–2100) scenarios. Lines represent annual values mean over 26 CMIP6 models. The shading is the 95% confidence intervals of 26 CMIP6 models. Two grey rectangular areas represent two time periods: 1950–2014 and 2070–2100. The right panel in **a-c**, attribution of changes in *AI* between 1950–2014 and 2070–2100 using the method described in [6]. Bars and error bars represent the ensemble mean and 95% confidence intervals of 26 CMIP6 models, respectively

projections from ecological and hydrological perspectives, i.e., projected global greening and runoff increasing.

Figures 2a-c right panels show the attribution of changes in *AI* between 1950–2014 and 2070–2100. In Fig. 2a, the cumulative negative effects of r_a, s, VPD, and R_n^* far outweigh the positive effect of precipitation (P), leading to a great decrease in *AI* (drying evolution). In Fig. 2b, the cumulative negative effects of r_a, s, VPD, and R_n^* slightly outweigh the cumulative positive effects of P and r_s (considering the influence of $[CO_2]$ on stomatal responses), leading to a slight decrease in *AI* (subtle drying evolution). In Fig. 2c, the cumulative negative effects of r_a, s, VPD, and R_n^* are outweighed by the cumulative positive effects of P and r_s (considering the influence of diverse environmental factors on stomatal responses), resulting in an increase in *AI* (wetting evolution). Given that $ET_{rc-Jarvis}$ can reconcile the conflicting aridity projections between aridity index and vegetation greenness as well as runoff projections, we confirm the deduction proposed by Roderick et al. [7] that ignoring stomatal responses is a key factor underlying the so-called 'aridity paradox'.

Drought Paradox

To assess the impact of neglecting stomatal responses on the emergence of the 'drought paradox', we choose the most widely used Palmer Drought Severity Index (*PDSI*) as a representative and calculate it using $ET_{rc-Jarvis}$, $ET_{rc-Yang}$, and ET_{rc}. *PDSI* is the most broadly used drought metric, accounting for changes in moisture supply (precipitation) and demand (*PET*) [69]. As a standardized drought metric, negative *PDSI* values and decreasing trends indicate drier-than-normal and intensifying drought conditions; conversely, positive values and increasing trends indicate wetter-than-normal and intensifying pluvial conditions. Resembling the calculation given by Yang et al. [39], annual drought frequency is estimated by the number of months with *PDSI*<-3 within a year, and annual drought extent is calculated by the areal coverage of grids experiencing drought within a year.

Figure 3a illustrates divergent *PDSI* trajectories projected by different stomatal quantifications. Annual *PDSI* values calculated using $ET_{rc-Jarvis}$ and $ET_{rc-Yang}$ exhibit upward trends, with more pronounced increases under higher greenhouse gas emission scenarios. The similar increases between $ET_{rc-Jarvis}$ and $ET_{rc-Yang}$ suggest that rising $[CO_2]$ is the dominant contributor to the *PDSI* trend, outweighing the influence of other environmental factors on stomata. In contrast, the series calculated by ET_{rc} shows a subtle downward tendency. The divergent trajectories highlight the critical role of stomatal responses to environmental changes when using indices such as *PDSI* to evaluate drought, and illustrate the emergence of the 'drought paradox'.

Unlike the annual *PDSI* series, projections for drought extent and frequency consistently show increasing trends under future scenarios across all stomatal quantifications (Fig. 3b and c). Compared to the results of ET_{rc}, incorporating the stomatal response to rising $[CO_2]$ reduces severe-drought-affected areas from 35% at the end of this century (Fig. 3b third column) to 25% under SSP585 and from 27 to 23% under SSP370 (Fig. 3b second column). When accounting for stomatal responses to multiple environmental variables, these ratios further decline to 22% and 20% (Fig. 3b first column), respectively. These differences indicate that, although stomatal responses cannot reverse the escalating trends in drought extent and frequency, they could benefit the pluvial conditions that, in turn, offset the increasing drought conditions from a global average perspective. Typically, *PDSI* values below -1, -2, and -3 indicate mild, moderate, and severe drought, respectively. To examine whether the choice of thresholds in calculating drought extent and frequency affects their increasing trends—as well as the dampening effects of stomatal responses on these trends—we replace -3 with -1 and -2 for uncertainty testing [39, 70]. The results show that while varying the thresholds alters the magnitude of the increases, the overall upward trends in extent and frequency persist, and the dampening effects of stomatal responses remain consistent.

According to differences in the Earth system variables and processes of interest, aridity and drought can be categorized from atmospheric/meteorologic, hydrologic, agricultural, and ecological perspectives [3, 25]. The multifaceted characteristics of aridity and drought have been widely accepted as the primary explanation of 'aridity and drought paradoxes' [3, 71]. In recent studies projecting aridity and dryland changes, nuanced multi-year mean runoff increase [54] suggests little change in hydrologic perspective, enhanced vegetation greenness and activity [72] indicate a wetting tendency in ecological perspective, while climbing vapor pressure deficit [73] as well as decreasing surface soil moisture [74] imply a drying trend in atmospheric and agricultural perspectives. In drought projections, although most studies anticipate more severe drought conditions in the future [75], drought trends and spatial patterns would be different or even opposite once considering different drought types (meteorologic, hydrologic, agricultural, and ecological) and characteristics (such as drought index trends versus frequency and extent) [76, 77]. Compared with the projections directly using the Earth system variables and processes, *PET*-based metrics contain characteristics from different perspectives, which makes the definition of these metrics ambiguous [78]. In addition, recent studies insist these metrics are redundant, as contemporary models and

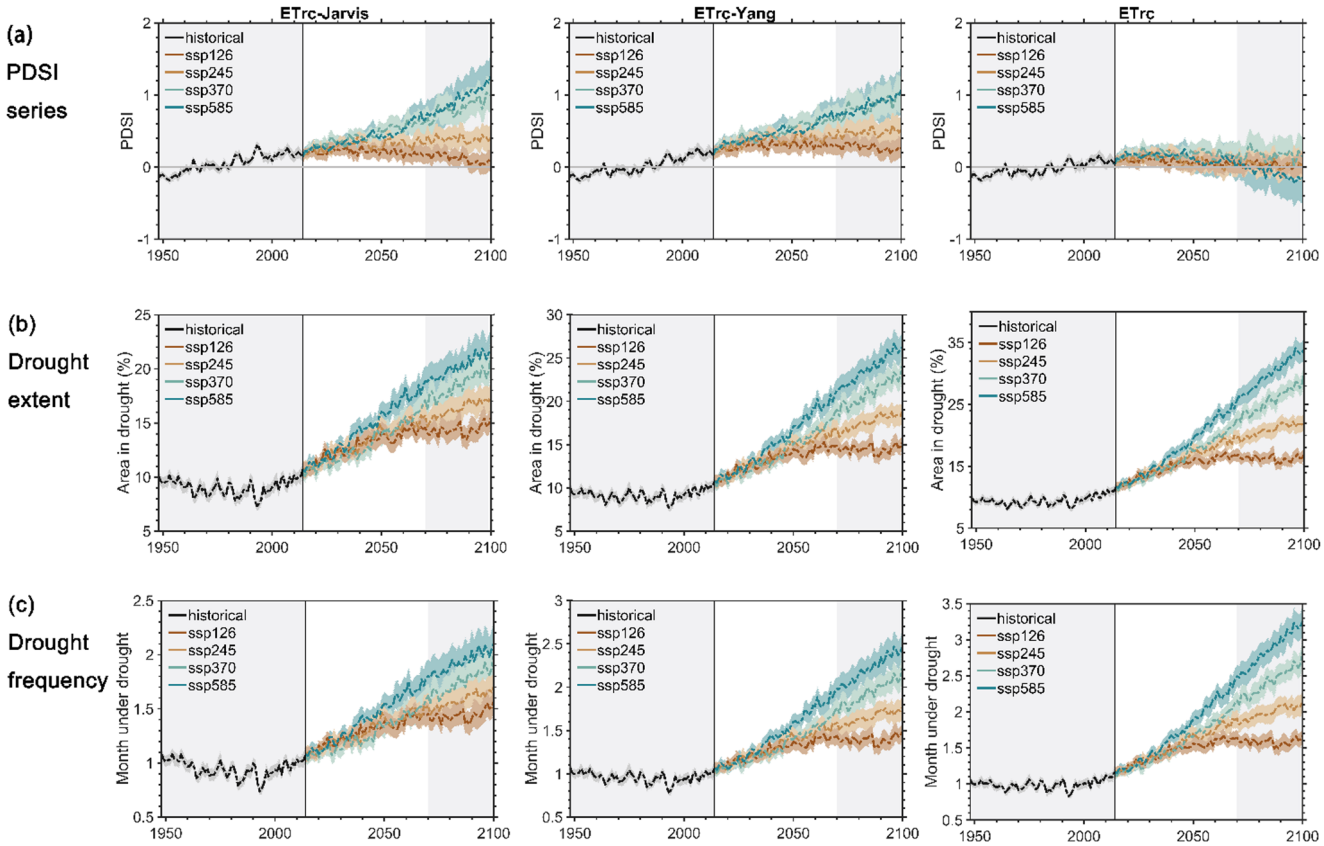

Fig. 3 Palmer Drought Severity Index (*PDSI*) series (**a**), along with its quantified drought extent (**b**) and frequency (**c**). In **a**, the y-axis represents *PDSI* anomalies over 1950–2100 relative to 1950–2014. **b** and **c** illustrate the extent and frequency experiencing severe drought (*PDSI*<-3). The first, second and third columns are respectively calculated by $ET_{rc-Jarvis}$, $ET_{rc-Yang}$ and ET_{rc}. Lines represent annual values mean over 26 CMIP6 models. The shading is the 95% confidence intervals of 26 CMIP6 models. Two grey rectangular areas represent two time periods: 1950–2014 and 2070–2100. As shown in Eq. (11), $ET_{rc-Jarvis}$ quantifies the effects of diverse environmental factors on stomatal responses. As shown in Eq. (5), $ET_{rc-Yang}$ quantifies the impact of rising [CO_2] on stomatal responses. By assuming fixed stomatal aperture and resistance, ET_{rc} neglects the stomatal changes

remote sensing algorithms can provide enough data to assess aridity and drought from different perspectives [26, 78]. Given the definitional ambiguity and redundancy, some studies suggest giving up using *PET*-based metrics.

We admit the issues underlying *PET*-based metrics, but argue they should not be discarded immediately. The most important reason is that worldwide dryland assessment as well as drought monitoring and warning have been built on these metrics, which have long histories of successful use and will continue to be used [20, 69]. Despite the emergence of massive reconstructed data on Earth system variables and processes, practical aridity and drought assessments still heavily rely on high-quality in-situ observations. In practice, there are vast regions without enough observations of ecohydrological variables, including evapotranspiration, soil moisture, and underground water. For aridity and drought assessment in these regions, combining densely distributed meteorological observations with *PET*-based metrics remains valuable. Summing up, it is foreseeable that using the reconstructed data on Earth system variables and processes for aridity and drought assessment is the trend with the development of Earth system models, but continuously correcting and updating previous metrics are still of great significance before establishing a complete and reliable observation network and simulation system.

Conclusions

Anthropogenic global warming significantly influences the hydrological cycle and complicates the formation and evolution of terrestrial water resources, thereby leaving severe challenges to the sustainable use of water resources. Recently, three ‘paradoxes’ associated with the evolution of water resources under global warming have emerged, namely the ‘evaporation paradox’ proposed around 2000 and the ‘aridity and drought paradoxes’ proposed around 2015. Despite these paradoxes stemming from various factors, the explanation of the ‘evaporation paradox’ and the calculation of aridity and

drought are all tied to *PET*. Therefore, this study reviews the emergence, development, and possible explanations of these paradoxes from the perspective of *PET*.

The emergence of a 'paradox' is primarily due to the limited understanding of related mechanisms during a certain period of time. The 'evaporation paradox' refers to the contradiction between the expected increase in atmospheric evaporative demand and the observed decrease in its observational proxy, pan evaporation. This limitation in understanding arose mainly from the unclear mechanisms of meteorological variables on pan evaporation before 2000. A consensus has been achieved with the development of physical models: before the mid-1990s, the enhancing effect of rising air temperature on pan evaporation is outweighed by the weakening effects of reduced radiation and declined wind speed. As climate warming continues after the mid-1990s, rising air temperature and downwelling longwave radiation are projected to drive upward trends in pan evaporation, indicating the paradox has disappeared and is unlikely to recur in a warming climate.

The 'aridity and drought paradoxes' refer to the conflicting drying and wetting projections in a warming climate. Neglecting stomatal responses in the calculation of potential evapotranspiration, which is the input for aridity and drought estimations, is deduced as the main reason underlying these conflicting projections. To analyze the impact of neglecting stomatal responses on these paradoxes, we compare three calculation methods: neglecting stomatal changes, accounting for the stomatal response to elevated [CO_2], and accounting for stomatal responses to diverse environmental factors, in the context of aridity and drought assessment. Neglecting stomatal changes in global aridity assessment projects a severely drying trend, while accounting for the stomatal response to elevated [CO_2] projects a slightly drying trend. Accounting for stomatal responses to diverse environmental factors projects a significantly wetting trend, which reconciles the conflicting aridity projections between the aridity index, vegetation greenness, and runoff projections. Therefore, we validate the deduction that ignoring stomatal responses in the traditional potential evapotranspiration calculation is a key factor underlying the 'aridity paradox'. Using the *PDSI* for drought assessment, we find that neglecting stomatal changes projects a decreasing annual *PDSI* trend, whereas accounting for various stomatal responses indicates increasing *PDSI* trends. However, unlike the projections of annual *PDSI*, considering stomatal responses cannot reverse the escalating trends in drought extent and frequency. Accordingly, we conclude that ignoring stomatal responses explains the paradoxical trends in drought indices but fails for drought extent and frequency.

Author Contributions K. W. and P. B. designed the review. K.W. wrote the main manuscript text and prepared Figs. 1, 2 and 3. P. B. and X. L. edited and reviewed the manuscript.

Funding This research was supported by the National Key Research and Development Program of China (Nos. 2023YFC3206600 and 2024YFC3013404), National Natural Science Foundation of China (Nos. 42271033 and 52209040), and China Association for Science and Technology Young Elite Scientist Sponsorship Program (No. YESS20220331).

Data Availability CMIP6 data used in Figs. 1, 2 and 3 were downloaded from the Word Climate Research Programme, and Global meteorological forcing data were provided by Princeton University.

Declarations

Competing Interests The authors declare no competing interests.

References

1. Oki T, Kanae S. Global hydrological cycles and world water resources. Science. 2006;313:1068–72.
2. Roderick ML, Farquhar GD. The cause of decreased Pan evaporation over the past 50 years. Science. 2002;298:1410–1.
3. Lian X, Piao S, Chen A, Huntingford C, Fu B, Li LZX, et al. Multifaceted characteristics of dryland aridity changes in a warming world. Nat Rev Earth Environ. 2021;2:232–50.
4. Trenberth KE, Dai A, van der Schrier G, Jones PD, Barichivich J, Briffa KR, et al. Global warming and changes in drought. Nat Clim Change. 2014;4:17–22.
5. Milly PCD, Dunne KA. Potential evapotranspiration and continental drying. Nat Clim Change. 2016;6:946–9.
6. Yang Y, Roderick ML, Zhang S, McVicar TR, Donohue RJ. Hydrologic implications of vegetation response to elevated CO2 in climate projections. Nat Clim Change. 2019;9:44–8.
7. Roderick ML, Greve P, Farquhar GD. On the assessment of aridity with changes in atmospheric CO $_2$. Water Resour Res. 2015;51:5450–63.
8. Miralles DG, Brutsaert W, Dolman AJ, Gash JH. On the use of the term evapotranspiration. Water Resour Res. 2020;56:e2020WR028055.
9. Yang Y, Roderick ML, Guo H, Miralles DG, Zhang L, Fatichi S, et al. Evapotranspiration on a greening Earth. Nat Rev Earth Environ. 2023;4:626–41.
10. Vicente-Serrano SM, McVicar TR, Miralles DG, Yang Y, Tomas-Burguera M. Unraveling the influence of atmospheric evaporative demand on drought and its response to climate change. WIREs Clim Change. 2020;11:e632.
11. Cook BI. Drought: an interdisciplinary perspective. New York: Columbia University; 2019.
12. McMahon TA, Peel MC, Lowe L, Srikanthan R, McVicar TR. Estimating actual, potential, reference crop and pan evaporation using standard meteorological data: a pragmatic synthesis. Hydrol Earth Syst Sci. 2013;17:1331–63.
13. Huang J, Li Y, Fu C, Chen F, Fu Q, Dai A, et al. Dryland climate change: recent progress and challenges: dryland climate change. Rev Geophys. 2017;55:719–78.
14. Hao Z, Yuan X, Xia Y, Hao F, Singh VP. An overview of drought monitoring and prediction systems at regional and global scales. Bull Am Meteorol Soc. 2017;98:1879–96.

15. AghaKouchak A, Mirchi A, Madani K, Di Baldassarre G, Nazemi A, Alborzi A, et al. Anthropogenic drought: definition, challenges, and opportunities. Rev Geophys. 2021;59:e2019RG000683.
16. Shyrokaya A, Pappenberger F, Pechlivanidis I, Messori G, Khatami S, Mazzoleni M, et al. Advances and gaps in the science and practice of impact-based forecasting of droughts. WIREs Water. 2024;11:e1698.
17. Peterson TC, Golubev VS, Groisman PY. Evaporation losing its strength. Nature. 1995;377:687–8.
18. Donohue RJ, McVicar TR, Roderick ML. Assessing the ability of potential evaporation formulations to capture the dynamics in evaporative demand within a changing climate. J Hydrol. 2010;386:186–97.
19. Wang K, Dickinson RE, Liang S. Global Atmospheric Evaporative Demand over Land from 1973 to 2008. 2012 [cited 2024 Nov 11]; Available from: https://journals.ametsoc.org/view/journals/clim/25/23/jcli-d-11-00492.1.xml
20. Cherlet M, Hutchinson C, Reynolds J, Hill J, Sommer S, von Maltitz G, editors. World Atlas of Desertification, Publication Office of the European Union, Luxembourg, 2018.
21. Huang J, Yu H, Guan X, Wang G, Guo R. Accelerated dryland expansion under climate change. Nat Clim Change. 2016;6:166–71.
22. Park C-E, Jeong S-J, Joshi M, Osborn TJ, Ho C-H, Piao S, et al. Keeping global warming within 1.5°C constrains emergence of aridification. Nat Clim Change. 2018;8:70–4.
23. Feng S, Gu X, Luo S, Liu R, Gulakhmadov A, Slater LJ et al. Greenhouse gas emissions drive global dryland expansion but not Spatial patterns of change in aridification. J Clim. 2022;35.
24. Berg A, McColl KA. No projected global drylands expansion under greenhouse warming. Nat Clim Change. 2021;11:331–7.
25. Zhang C, Yang Y, Yang D, Wu X. Multidimensional assessment of global dryland changes under future warming in climate projections. J Hydrol. 2021;592:125618.
26. Greve P, Roderick ML, Ukkola AM, Wada Y. The aridity index under global warming. Environ Res Lett. 2019;14:124006.
27. Scheff J, Mankin S, Coats J, Liu S. CO_2 -plant effects do not account for the gap between dryness indices and projected dryness impacts in CMIP6 or CMIP5. Environ Res Lett. 2021;16:034018.
28. Mishra AK, Singh VP. A review of drought concepts. J Hydrol. 2010;391:202–16.
29. Mukherjee S, Mishra A, Trenberth KE. Climate change and drought: a perspective on drought indices. Curr Clim Change Rep. 2018;4:145–63.
30. Van Loon AF. Hydrological drought explained. WIREs Water. 2015;2:359–92.
31. Pokhrel Y, Felfelani F, Satoh Y, Boulange J, Burek P, Gädeke A, et al. Global terrestrial water storage and drought severity under climate change. Nat Clim Change. 2021;11:226–33.
32. Wells N, Goddard S, Hayes MJ, A Self-Calibrating Palmer Drought Severity Index. 2004 [cited 2024 Nov 18]; Available from: https://journals.ametsoc.org/view/journals/clim/17/12/1520-0442_2004_017_2335_aspdsi_2.0.co_2.xml
33. Vicente-Serrano SM, Beguería S, López-Moreno JI. A Multiscalar drought index sensitive to global warming: the standardized precipitation evapotranspiration index. 2010 [cited 2024 Nov 18]; Available from: https://journals.ametsoc.org/view/journals/clim/23/7/2009jcli2909.1.xml
34. Dai A. Increasing drought under global warming in observations and models. Nat Clim Change. 2013;3:52–8.
35. Liu W, Sun F, Lim WH, Zhang J, Wang H, Shiogama H, et al. Global drought and severe drought-affected populations in 1.5 and 2°C warmer worlds. Earth Syst Dyn. 2018;9:267–83.
36. Dai A. Hydroclimatic trends during 1950–2018 over global land. Clim Dyn. 2021;56:4027–49.
37. Chiang F, Mazdiyasni O, AghaKouchak A. Evidence of anthropogenic impacts on global drought frequency, duration, and intensity. Nat Commun. 2021;12:2754.
38. Sheffield J, Wood EF, Roderick ML. Little change in global drought over the past 60 years. Nature. 2012;491:435–8.
39. Yang Y, Zhang S, Roderick ML, McVicar TR, Yang D, Liu W, et al. Comparing Palmer drought severity index drought assessments using the traditional offline approach with direct climate model outputs. Hydrol Earth Syst Sci. 2020;24:2921–30.
40. Cook BI, Mankin JS, Anchukaitis KJ. Climate change and drought: from past to future. Curr Clim Change Rep. 2018;4:164–79.
41. Elie M. Toward a complex socio-environmental Understanding of drought: the contribution of the social sciences and humanities. WIREs Clim Change. 2024;15:e907.
42. Thom AS, Thony J-L, Vauclin M. On the proper employment of evaporation pans and atmometers in estimating potential transpiration. Q J R Meteorol Soc. 1981;107:711–36.
43. Pereira AR, Villa Nova NA, Pereira AS, Barbieri V. A model for the class A pan coefficient. Agric Meteorol. 1995;76:75–82.
44. Linacre ET, Estimating US, Class. A Pan evaporation from few climate data. Water Int. 1994;19:5–14.
45. Rotstayn LD, Roderick ML, Farquhar GD. A simple pan-evaporation model for analysis of climate simulations: Evaluation over Australia. Geophys Res Lett [Internet]. 2006 [cited 2024 Nov 18];33. Available from: https://onlinelibrary.wiley.com/doi/abs/https://doi.org/10.1029/2006GL027114
46. Lim WH, Roderick ML, Farquhar GD. A mathematical model of pan evaporation under steady state conditions. J Hydrol. 2016;540:641–58.
47. Yang H, Yang D. Climatic factors influencing changing pan evaporation across China from 1961 to 2001. J Hydrol. 2012;414:184–93.
48. Wang K, Liu X, Tian W, Li Y, Liang K, Liu C, et al. Pan coefficient sensitivity to environment variables across China. J Hydrol. 2019;572:582–91.
49. Wang K, Liu X, Li Y, Liu C, Yang X. A generalized evaporation model for Chinese pans. J Geophys Res Atmos. 2018;123:10943–66.
50. Wild M, Gilgen H, Roesch A, Ohmura A, Long CN, Dutton EG, et al. From dimming to brightening: decadal changes in solar radiation at earth's surface. Science. 2005;308:847–50.
51. McVicar TR, Roderick ML, Donohue RJ, Li LT, Van Niel TG, Thomas A, et al. Global review and synthesis of trends in observed terrestrial near-surface wind speeds: implications for evaporation. J Hydrol. 2012;416–417:182–205.
52. Roderick ML, Hobbins MT, Farquhar GD. Pan evaporation trends and the terrestrial water balance. II. Energy balance.and interpretation. Geogr Compass. 2009;3:761–80.
53. Wang K, Liu X, Liu C, Yang X, Bai P, Li Y, et al. The unignorable impacts of pan wall on pan evaporation dynamics. Agric Meteorol. 2019;274:42–50.
54. IPCC. Summary for policymakers. In: Lee H, Romero J, editors. Climate change 2023: synthesis report.contribution of working groups I, II and III to the sixth assessment report of the intergovernmental panel on climate change [Core Writing Team. Geneva, Switzerland: IPCC; 2023. pp. 1–34. https://doi.org/10.59327/IPCC/AR6-9789291691647.001.
55. Zeng Z, Ziegler AD, Searchinger T, Yang L, Chen A, Ju K, et al. A reversal in global terrestrial stilling and its implications for wind energy production. Nat Clim Change. 2019;9:979–85.
56. Cohen S, Stanhill G. Chapter 32 - Changes in the Sun's radiation: the role of widespread surface solar radiation trends in climate change: dimming and brightening. In: Letcher TM, editor. Clim Change Third Ed [Internet]. Elsevier; 2021 [cited 2024 Nov 18]. pp. 687–709. Available from: https://www.sciencedirect.com/science/article/pii/B9780128215753000323

57. Wild M, Wacker S, Yang S, Sanchez-Lorenzo A. Evidence for Clear-Sky dimming and brightening in central Europe. Geophys Res Lett. 2021;48:e2020GL092216.
58. Stephens CM, McVicar TR, Johnson FM, Marshall LA. Revisiting Pan evaporation trends in Australia a decade on. Geophys Res Lett. 2018;45:11,164–11,172.
59. Wang K, Liu X, Li Y, Yang X, Bai P, Liu C, et al. Deriving a long-term pan evaporation reanalysis dataset for two Chinese pan types. J Hydrol. 2019;579:124162.
60. Mozny M, Trnka M, Vlach V, Vizina A, Potopova V, Zahradnicek P, et al. Past (1971–2018) and future (2021–2100) pan evaporation rates in the Czech Republic. J Hydrol. 2020;590:125390.
61. Shen J, Yang H, Li S, Liu Z, Cao Y, Yang D. Revisiting the Pan evaporation trend in China during 1988–2017. J Geophys Res Atmos. 2022;127:e2022JD036489.
62. Sheffield J, Goteti G, Wood EF. Development of a 50-Year High-Resolution global dataset of meteorological forcings for land surface modeling. J Clim. 2006;19:3088–111.
63. Allen RG, Pereira LS, Raes D, Smith M. Crop Evapotranspiration Guidelines for Computing Crop Water Requirements FAO Irrigation and Drainage Paper No. 56. 1998.
64. Damour G, Simonneau T, Cochard H, Urban L. An overview of models of stomatal conductance at the leaf level: models of stomatal conductance. Plant Cell Environ. 2010;no-no.
65. Piao S, Wang X, Park T, Chen C, Lian X, He Y, et al. Characteristics, drivers and feedbacks of global greening. Nat Rev Earth Environ. 2020;1:14–27.
66. Jarvis PG. The interpretation of the variations in leaf water potential and stomatal conductance found in canopies in the field. Philos Trans R Soc Lond B Biol Sci. 1976;273:593–610.
67. Dickinson RE, Henderson-Sellers A, Kennedy PJ. (1993). Biosphere-atmosphere Transfer Scheme (BATS) Version 1e as Coupled to the NCAR Community Climate Model (No. NCAR/TN-387+STR). University Corporation for Atmospheric Research. https://doi.org/10.5065/D67W6959
68. Kumar A, Chen F, Niyogi D, Alfieri JG, Ek M, Mitchell K. Evaluation of a Photosynthesis-Based canopy resistance formulation in the Noah Land-Surface model. Bound-Layer Meteorol. 2011;138:263–84.
69. Hao Z, Singh VP, Xia Y. Seasonal drought prediction: advances, challenges, and future prospects. Rev Geophys. 2018;56:108–41.
70. Li X, Wang K, Liu C, Zhao G, Jiang Z, Luo Q, et al. Exacerbating hydrological extremes in china's large reservoir drainage areas. J Hydrol. 2025;659:133297.
71. Cook BI, Mankin JS, Marvel K, Williams AP, Smerdon JE, Anchukaitis KJ. Twenty-First Century Drought Projections in the CMIP6 Forcing Scenarios. Earths Future [Internet]. 2020 [cited 2022 Dec 6];8. Available from: https://onlinelibrary.wiley.com/doi/https://doi.org/10.1029/2019EF001461
72. Chen C, Park T, Wang X, Piao S, Xu B, Chaturvedi RK, et al. China and India lead in greening of the world through land-use management. Nat Sustain. 2019;2:122–9.
73. Yuan W, Zheng Y, Piao S, Ciais P, Lombardozzi D, Wang Y, et al. Increased atmospheric vapor pressure deficit reduces global vegetation growth. Sci Adv. 2019;5:eaax1396.
74. Berg A, Sheffield J, Milly PCD. Divergent surface and total soil moisture projections under global warming. Geophys Res Lett. 2017;44:236–44.
75. Seneviratne SI, Zhang X, Adnan M, Badi W, Dereczynski C, Di Luca A, Ghosh S, Iskandar I, Kossin J, Lewis S, Otto F, Pinto I, Satoh M, Vicente-Serrano SM, Wehner M, Zhou B. Weather and Climate Extreme Events in a Changing Climate. In: Delmotte V, Zhai P, Pirani A, Connors SL, Péan C, Berger S, Caud N, Chen Y, Goldfarb L, Gomis MI, Huang M, Leitzell K, Lonnoy E, Matthews JBR, Maycock TK, Waterfield T, Yelekçi O, Yu R, Zhou B, editors. Climate Change 2021: The Physical Science Basis. Cambridge, United Kingdom and New York, NY, USA: Cambridge University Press; 2021. pp. 1513–766. https://doi.org/10.1017/9781009157896.013. Contribution of Working Group I to the Sixth Assessment Report of the Intergovernmental Panel on Climate Change [Masson-.
76. Swann ALS, Hoffman FM, Koven CD, Randerson JT. Plant responses to increasing CO_2 reduce estimates of climate impacts on drought severity. Proc Natl Acad Sci. 2016;113:10019–24.
77. Ukkola AM, De Kauwe MG, Roderick ML, Abramowitz G, Pitman AJ. Robust Future changes in meteorological drought in CMIP6 projections despite uncertainty in precipitation. Geophys Res Lett [Internet]. 2020 [cited 2022 Dec 6];47. Available from: https://doi.org/10.1029/2020GL087820https://onlinelibrary.wiley.com/doi/
78. McColl KA, Roderick ML, Berg A, Scheff J. The terrestrial water cycle in a warming world. Nat Clim Change. 2022;12:604–6.